

Diffraction effects of telescope secondary mirror spiders on various image-quality criteria

James E. Harvey and Christ Ftaclas

Diffraction from secondary mirror spiders can significantly affect the image quality of optical telescopes; however, these effects vary drastically with the chosen image-quality criterion. Rigorous analytical calculations of these diffraction effects are often unwieldy, and virtually all commercially available optical design and analysis codes that have a diffraction-analysis capability are based on numerical Fourier-transform algorithms that frequently lack an adequate sampling density to model narrow spiders. The effects of spider diffraction on the Strehl ratio (or peak intensity of the diffraction image), full width at half-maximum of the point-spread function, the fractional encircled energy, and the modulation transfer function are discussed in detail. A simple empirical equation is developed that permits accurate engineering calculations of fractional encircled energy for an arbitrary obscuration ratio and spider configuration. Performance predictions are presented parametrically in an attempt to provide insight into this sometimes subtle phenomenon.

Key words: Spider diffraction, telescope diffraction effects, image-quality criteria.

1. Introduction

The qualitative effect of secondary-mirror spiders on the image-intensity distribution or point-spread function (PSF) of an optical telescope is well known to every amateur astronomer who has observed the familiar diffraction spikes accompanying star images as shown in Figs. 1(a) and 1(c). These effects can be important in certain scientific applications, depending on the image-quality criterion. However, more attention seems to have been devoted to this problem by amateur astronomers than by scientists and engineers. Several discussions concerning the use of curved spiders to reduce or eliminate these objectionable diffraction spikes have been reported by amateur astronomers.¹⁻⁵ These include a diffractionless mount that is achieved by merely attaching the secondary mirror to a section of pipe that is then attached to the telescope structure. Indeed the resulting star images are devoid of the objectionable diffraction spikes, as illustrated in Fig. 1(b). Another

amateur astronomer reported on an antidiffraction mask for a telescope that effectively eliminated the diffraction spikes at a considerable reduction in collecting area.⁶ Curved spider configurations similar to those shown in Fig. 1(d) that do not produce prominent diffraction spikes are also available commercially.⁷ Clearly diffraction effects that can degrade the image still exist; however, the azimuthal variations in the image-intensity distribution have been eliminated. Whether this results in a superior image depends on the application and the appropriate image-quality criterion for that application. Only four references have been found in the professional technical literature that deal specifically with spider diffraction.⁸⁻¹¹ Several additional papers were found that deal with the more general subject of aperture configurations but include a peripheral discussion of spider diffraction effects.¹²⁻¹⁵ Incidentally, the images shown in Fig. 1 were actual photographs taken in a laboratory setup where different masks were illuminated with laser light. Note the detailed structure in the images. This structure is also a diffraction (or interference) effect produced by the aperture and is discussed below.

2. Image-Quality Criteria

If visual aesthetics is the chosen image-quality criterion, or if one is trying to observe bright binary stars visually, the curved spiders that eliminate diffraction spikes are probably desirable. However, the diffrac-

J. E. Harvey is with the Center for Research and Education in Optics and Lasers, The University of Central Florida, 12424 Research Parkway, Orlando, Florida 32826. Christ Ftaclas is with Hughes Danbury Optical Systems, Inc., 100 Wooster Heights Road, M/S 813, Danbury, Connecticut 06810.

Received 19 December 1994; revised manuscript received 13 March 1995.

0003-6935/95/286337-13\$06.00/0.

© 1995 Optical Society of America.

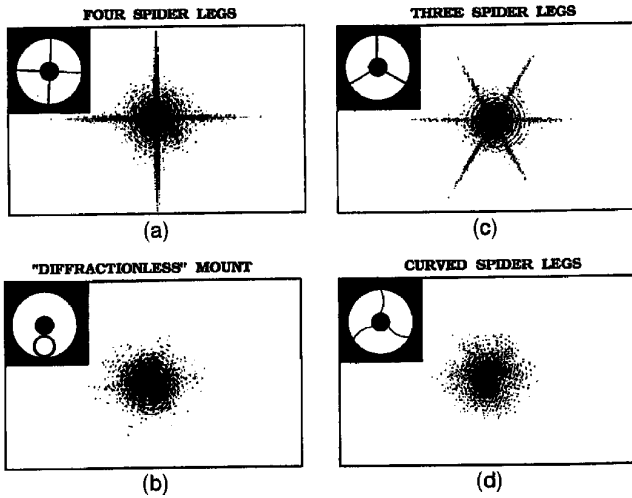


Fig. 1. Diffraction effects of secondary mirror spiders on telescope image quality.

tion spikes caused by conventional (narrow) spiders do not significantly broaden the image core. The full width at half-maximum (FWHM) of the PSF, an appropriate image-quality criterion when bright point sources are observed, is therefore not degraded by diffraction effects from secondary mirror spiders. This FWHM has been the astronomers' classical definition of resolution. Perhaps this explains the apparent lack of concern about this subject as evidenced by the small number of technical papers in the literature.

The complex pupil function describes the amplitude (aperture shape including obscurations and spider configuration) and phase (wave-front aberrations) variations in the exit pupil of the telescope that determine image quality. Wave-front aberrations (which are neglected in this discussion of diffraction effects) are rendered observable and measured by interferometric techniques. Single-number merit functions derivable from interferometric data include

the rms wave-front error and the peak-to-valley wave-front error.

The PSF is the squared modulus of the Fourier transform of the complex pupil function as illustrated in Fig. 2.¹⁶ The intermediate quantity called the amplitude spread function is not an observable quantity with ordinary sensors. Frequently used single-number merit functions (or image-quality criteria) obtained from the PSF are the resolution (FWHM), the Strehl ratio, and the fractional encircled energy. Fractional encircled energy, or the closely related half-power radius, of the PSF have become common image-quality requirements imposed on telescope manufacturers in recent years. These image-quality criteria are particularly relevant if the telescope is to be used to collect light and place the image on the slit of a spectrographic instrument.

The autocorrelation theorem of Fourier-transform theory permits us to define the optical transfer function (OTF) as the normalized autocorrelation of the complex pupil function. Various properties of the OTF, or its modulus, the modulation transfer function, may provide more appropriate image-quality criteria if the application involves studying fine detail in extended objects. Limiting resolution and the transfer factor at a specific spatial frequency are single-number merit functions derivable from the OTF.

In the remainder of this paper we deal quantitatively with diffraction effects of secondary mirror spiders on several different image-quality criteria including the Strehl ratio, the fractional encircled energy, and the modulation transfer function.

3. Strehl Ratio

The Strehl ratio, defined as the ratio of the peak irradiance of an aberrated PSF to the peak irradiance of the diffraction-limited PSF, is a commonly used image-quality criterion. A slight modification of this definition (the diffraction-limited peak irradiance with spiders divided by the diffraction-limited peak irradi-

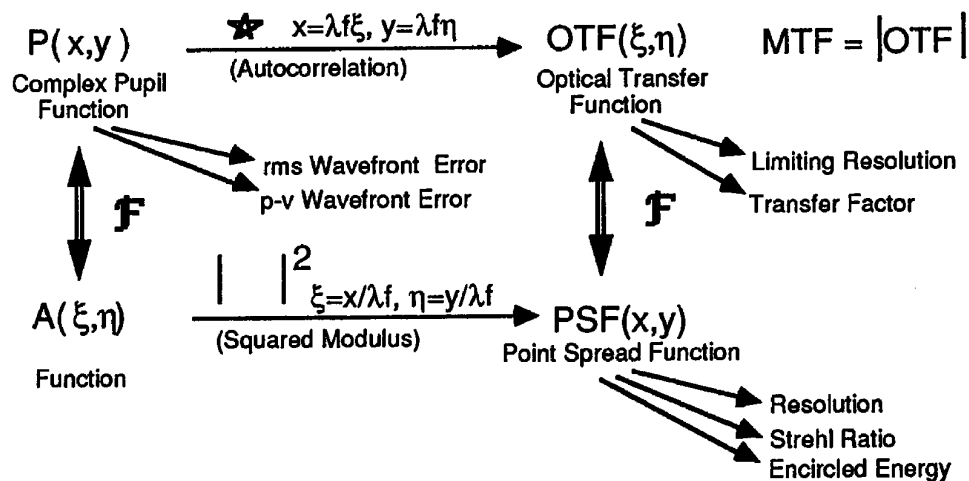


Fig. 2. Relationship among the complex pupil function, the PSF, and the OTF. Frequently used image-quality criteria associated with each function are indicated.

ance without spiders) is appropriate for this study. From the central ordinate theorem of the Fourier-transform theory (which states that the area of a function is equal to the central ordinate of its Fourier transform)¹⁷ and the relationships shown in Fig. 2, it is clear that the Strehl ratio can be expressed as

$$\text{Strehl ratio} \equiv S = \left(\frac{A_{\text{annulus}} - A_{\text{spiders}}}{A_{\text{annulus}}} \right)^2, \quad (1)$$

where A_{annulus} is the area of the annular aperture without spiders and A_{spiders} is the total area of all spiders. For any number N of straight radial spiders of width δD in an annular aperture of linear obscuration ratio ϵ , we can write

$$A_{\text{annulus}} = \pi D^2(1 - \epsilon^2)/4, \quad (2)$$

$$A_{\text{spiders}} = ND^2\delta(1 - \epsilon)/2, \quad (3)$$

$$S = \left[1 - \frac{2N\delta}{\pi(1 + \epsilon)} \right]^2. \quad (4)$$

This expression, and indeed the discussion throughout this paper, requires that the spiders be thin compared with the central obscuration ($\delta \ll \epsilon$).

Figure 3 is a parametric plot of the Strehl ratio for the case of four spiders as a function of the spider width for a variety of obscuration ratios.

For an obscuration ratio $\epsilon = 0.20$ and four spiders of fractional width $\delta = 0.03$, we thus obtain a Strehl ratio of ~ 0.88 as highlighted in Fig. 3.

4. Fractional Encircled Energy

The complex amplitude distribution in the focal plane of a telescope is given by the product of some complex exponentials with the Fourier transform of the complex pupil function evaluated at spatial frequencies $\xi = x_2/\lambda f$ and $\eta = y_2/\lambda f$.¹⁶

$$U(x_2, y_2) = \frac{\exp(ikf)}{i\lambda f} \exp\left[\frac{i\pi(x_2^2 + y_2^2)}{\lambda f}\right] \times \mathcal{F}\{U_1(x_1, y_1)\}_{\xi=x_2/\lambda f, \eta=y_2/\lambda f} \quad (5)$$

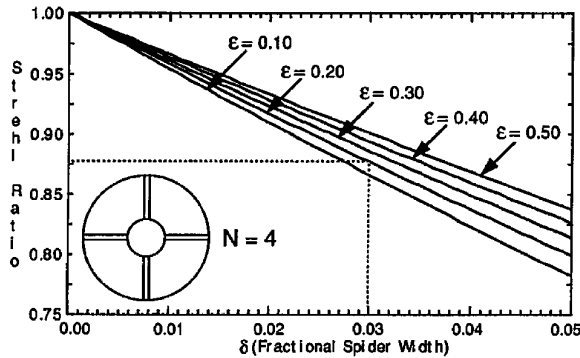


Fig. 3. Parametric plot of the ratio of the peak irradiance in the diffraction-limited PSF produced by an annular aperture of obscuration ratio ϵ and four spiders of width δD divided by that produced by an annular aperture without spiders.

Here $k = (2\pi)/\lambda$, f is the focal length of the telescope, \mathcal{F} denotes the Fourier-transform operation, and the complex pupil function is given by

$$U_1(x_1, y_1) = B(x_1, y_1)T_1(x_1/D, y_1/D)\exp[ikW(x_1, y_1)], \quad (6)$$

where $B(x_1, y_1)$ is the incident amplitude distribution (field strength), $T_1(x_1/D, y_1/D)$ is the aperture function of outer diameter D (including any obscurations of spiders), and $W(x_1, y_1)$ is the wave-front aberration function¹⁸ describing any phase variations in the exit pupil of the telescope.

For a uniform amplitude, normally incident plane wave (no aberrations), the pupil function is just the constant B times the aperture function,

$$U_1(x_1, y_1) = BT_1(x_1/D, y_1/D), \quad (7)$$

and the irradiance distribution in the image plane illustrated in Fig. 4 is given by

$$I(x_2, y_2) = |U(x_2, y_2)|^2 = \frac{B^2}{\lambda^2 f^2} \left| \mathcal{F}\left\{T_1\left(\frac{x_1}{D}, \frac{y_1}{D}\right)\right\}_{\xi=x_2/\lambda f, \eta=y_2/\lambda f} \right|^2. \quad (8)$$

By applying the central ordinate theorem of the Fourier transform theory to Eq. (8), we see that the on-axis irradiance in the image plane is given by

$$I(0, 0) = \frac{B^2}{\lambda^2 f^2} A_{\text{aperture}}^2. \quad (9)$$

The normalized irradiance distribution (normalized to unity at the origin) is thus expressed in dimensionless coordinates $x = x_2 D/\lambda f$ and $y = y_2 D/\lambda f$ as

$$I_n(x, y) = \frac{I(x_2, y_2)}{I(0, 0)} = \frac{1}{A_{\text{aperture}}^2} \left| \mathcal{F}\left\{T_1\left(\frac{x_1}{D}, \frac{y_1}{D}\right)\right\}_{\xi=x_2/\lambda f, \eta=y_2/\lambda f} \right|^2, \quad (10)$$

where A_{aperture} is just the area of the aperture.

The fractional encircled energy, a commonly used image-quality criterion, is defined as the radiant energy contained in a circle of radius r_2 divided by the

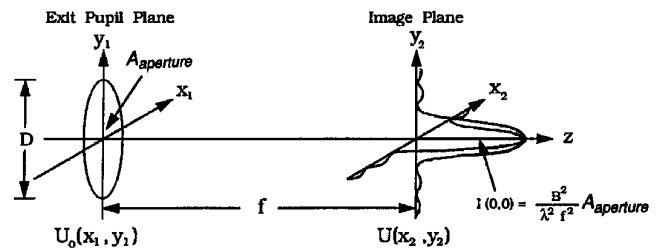


Fig. 4. Diffraction-limited irradiance distribution in the focal plane of a telescope depending on the dimensions of the pupil function in the exit pupil, the focal length of the telescope, the wavelength, and the incident field strength.

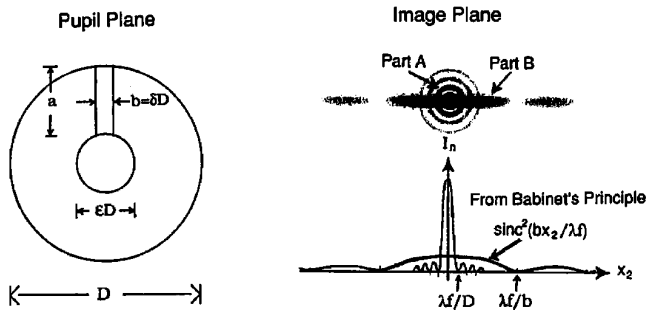


Fig. 5. Diffraction-limited PSF for an annular aperture with a narrow opaque strut consisting of two parts: an image core and a diffraction flare perpendicular to the strut.

total radiant energy reaching the focal plane:

$$EE(r_2) = \frac{\int_{\phi=0}^{2\pi} \int_{r=0}^r I(x_2, y_2) r_2 dr_2 d\phi}{\int_{x_2=0}^{\infty} \int_{y_2=0}^{\infty} I(x_2, y_2) dx_2 dy_2} \quad (11)$$

Substituting Eq. (8), we see that the denominator of Eq. (11) can be written as

$$\int_{x_2=0}^{\infty} \int_{y_2=0}^{\infty} I(x_2, y_2) dx_2 dy_2 = \frac{B^2}{\lambda^2 f^2} \int_{x_2=0}^{\infty} \int_{y_2=0}^{\infty} \left| \mathcal{F} \left[T_1 \left(\frac{x_1}{D}, \frac{y_1}{D} \right) \right] \right|_{\xi=x_2/\lambda f, \eta=y_2/\lambda f}^2 \times \lambda^2 f^2 d\xi d\eta, \quad (12)$$

and when Rayleigh's theorem is applied,^{17,19} which states that the integral of the squared modulus of a function is equal to the integral of the squared modulus of its Fourier transform (which corresponds to Parseval's theorem for the Fourier series), Eq. (12)

is equal to

$$\int_{x_2=0}^{\infty} \int_{y_2=0}^{\infty} I(x_2, y_2) dx_2 dy_2 = B^2 \int_{x_1=0}^{\infty} \int_{y_1=0}^{\infty} \left| T_1 \left(\frac{x_1}{D}, \frac{y_1}{D} \right) \right|^2 \times dx_1 dy_1. \quad (13)$$

But for a binary amplitude aperture that has a transmittance of either unity or zero,

$$\left| T_1 \left(\frac{x_1}{D}, \frac{y_1}{D} \right) \right|^2 = T_1 \left(\frac{x_1}{D}, \frac{y_1}{D} \right). \quad (14)$$

Hence the denominator of Eq. (11) can be written as

$$\int_{x_2=0}^{\infty} \int_{y_2=0}^{\infty} I(x_2, y_2) dx_2 dy_2 = B^2 A_{\text{aperture}}. \quad (15)$$

Now, substituting

$$I(x_2, y_2) = \frac{B^2 A_{\text{aperture}}^2}{\lambda^2 f^2} I_n(x, y) \quad (16)$$

into the numerator of Eq. (11) and noting that $r = r_2 D / \lambda f$ and $dr = dr_2 D / \lambda f$ in dimensionless coordinates, we obtain the fractional encircled energy in terms of the normalized irradiance distribution:

$$EE(r) = \frac{A_{\text{aperture}}}{D^2} \int_{\phi=0}^{2\pi} \int_{r=0}^r I_n(x, y) r dr d\phi. \quad (17)$$

The difficulty comes in obtaining the Fourier transform of the aperture function in Eq. (10) for arbitrary spider configurations. There are two choices. The Fourier transform of the aperture function can be obtained analytically or numerically. In this day of fast and inexpensive computers and many commercially available optical-analysis codes, the numerical approach seems to be the obvious choice. However, virtually all the commercially available optical-design

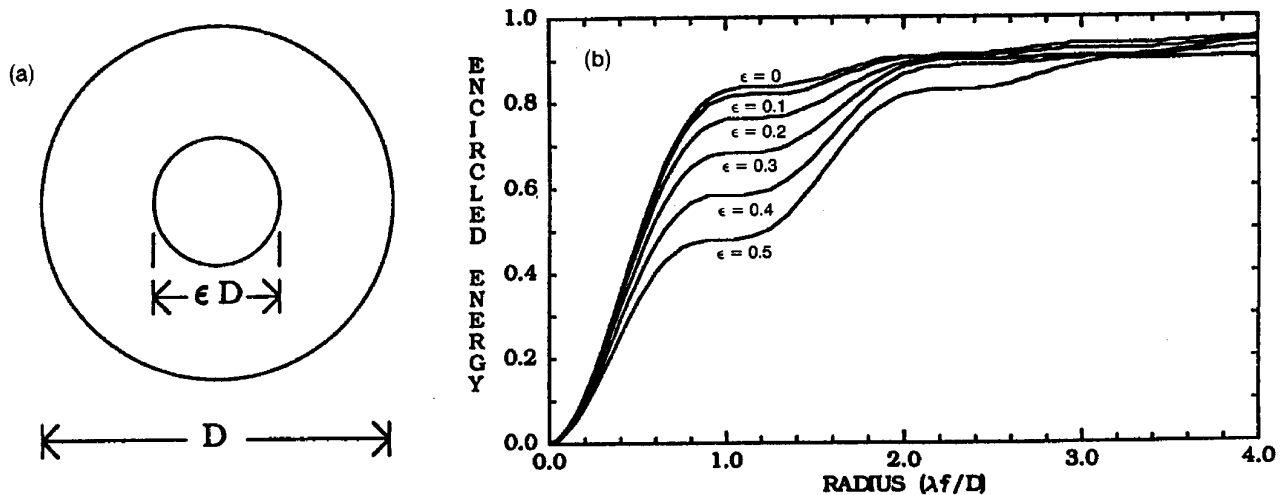


Fig. 6. Encircled energy caused by the diffraction-limited annular apertures. This figure can be used as a set of characteristic curves from which to obtain values of $EE_{\text{annulus}}(r)$, which are necessary when the empirical equation is applied to various aperture configurations.

Table 1. Fractional Encircled Energy from Diffraction-Limited Annular Apertures

Radius ($r_2 D / \lambda f$)	Fractional Encircled Energy					
	$\epsilon = 0.0$	$\epsilon = 0.1$	$\epsilon = 0.2$	$\epsilon = 0.3$	$\epsilon = 0.4$	$\epsilon = 0.5$
0.00	0.0000	0.0000	0.0000	0.0000	0.0000	0.0000
0.20	0.1031	0.1020	0.0988	0.0934	0.0858	0.0763
0.40	0.3381	0.3340	0.3218	0.3018	0.2746	0.2406
0.60	0.5587	0.5801	0.5546	0.5136	0.4588	0.3930
0.80	0.7592	0.7455	0.7055	0.6424	0.5612	0.4677
1.00	0.8281	0.8103	0.7592	0.6809	0.5843	0.4787
1.20	0.8379	0.8185	0.7639	0.6835	0.5891	0.4913
1.40	0.8424	0.8245	0.7755	0.7069	0.6309	0.5544
1.60	0.8638	0.8497	0.8129	0.7650	0.7146	0.6594
1.80	0.8909	0.8815	0.8587	0.8324	0.8037	0.7586
2.00	0.9069	0.9011	0.8894	0.8789	0.8620	0.8143
2.20	0.9100	0.9058	0.8996	0.8971	0.8831	0.8283
2.40	0.9112	0.9065	0.9004	0.8995	0.8853	0.8296
2.60	0.9186	0.9116	0.9022	0.9002	0.8875	0.8417
2.80	0.9293	0.9195	0.9058	0.9027	0.8944	0.8654
3.00	0.9362	0.9242	0.9075	0.9041	0.9006	0.8876
3.20	0.9377	0.9249	0.9078	0.9043	0.9027	0.8990
3.40	0.9383	0.9263	0.9116	0.9072	0.9028	0.9015
3.60	0.9240	0.9322	0.9215	0.9146	0.9041	0.9016
3.80	0.9476	0.9406	0.9342	0.9233	0.9060	0.9025
4.00	0.9515	0.9468	0.9435	0.9284	0.9067	0.9032
4.20	0.9524	0.9489	0.9471	0.9294	0.9071	0.9033
4.40	0.9527	0.9490	0.9474	0.9301	0.9109	0.9042
4.60	0.9549	0.9500	0.9480	0.9342	0.9196	0.9067
4.80	0.9584	0.9518	0.9496	0.9408	0.9300	0.9092
5.00	0.9609	0.9530	0.9507	0.9465	0.9371	0.9100

and -analysis codes that do have a diffraction-analysis capability are based on numerical Fourier-transform algorithms that lack adequate sampling density to model narrow spiders.

There must be several numerical samples across the width of the spider if the code is to predict $I_n(x, y)$ accurately. Suppose we require three samples across a spider whose width is 1% of the aperture diameter. This implies 300 samples across the aperture. A

50% guard band to prevent aliasing would then require at least a 600×600 numerical array. This is larger than can be conveniently handled by many computers.

Also, the normalization must be performed properly. Fractional encircled energy is just that, a fraction. It has a numerator and a denominator. It is not sufficient to calculate the numerator accurately. One must then divide by the proper denominator. The denominator is merely the total energy reaching the focal plane. One commercially available code merely adds up the energy in the first seven Airy rings and divides by that value.²⁰ This technique is adequate for clear annular apertures without a high-spatial-frequency structure; however, if a small percent of the energy is diffracted into wide angles by narrow struts or spiders, erroneously encircled energy predictions result.

The problems above can lead to one of several unfortunate situations: (a) The user may ignore spider diffraction altogether and thus impose image-quality requirements that are physically unobtainable. (b) The user may think the diffraction effects of spiders are being accurately modeled when in fact they are not. (c) The user may be aware of the sampling problem and thus try to model the effects of spiders by merely increasing the central obscuration to account for the additional obscuration caused by the spiders. It will presently become clear why this latter situation is not a good approximation to actually modeling the diffraction behavior of narrow spiders.

These problems led us to develop a code that employs a hybrid technique for making encircled energy predictions in the presence of narrow secondary mirror spiders. For any number of straight spiders lying along the radius of the aperture, we obtain the Fourier transform of the pupil function analytically to obtain the normalized irradiance distribution. We then perform a numerical integration

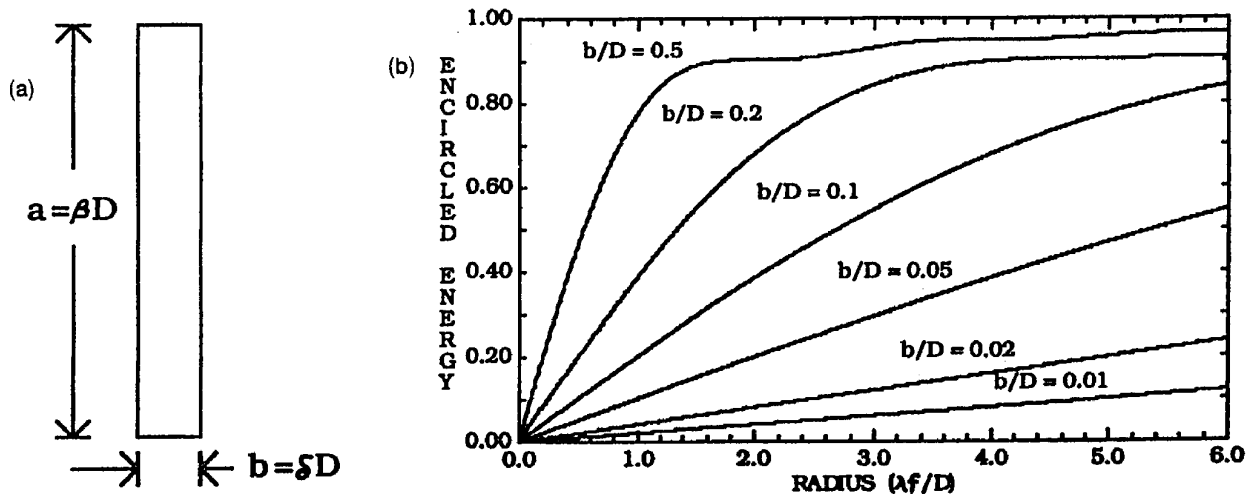


Fig. 7. Fractional encircled energy resulting from diffraction-limited narrow rectangular apertures. This figure can be used as a set of characteristic curves from which to obtain values of $EE_{\text{rect}}(r)$, which are necessary when the empirical equation is applied to various aperture configurations.

Table 2. Fractional Encircled Energy from Narrow Rectangular Apertures

Radius ($r_2 D / \lambda f$)	Fractional Encircled Energy					
	$\delta = 0.01$	$\delta = 0.02$	$\delta = 0.05$	$\delta = 0.10$	$\delta = 0.20$	$\delta = 0.50$
0.00	0.0003	0.0006	0.0015	0.0029	0.0052	0.0050
0.20	0.0043	0.0086	0.0215	0.0429	0.0851	0.2027
0.40	0.0083	0.0166	0.0415	0.0828	0.1641	0.3874
0.60	0.0123	0.0246	0.0614	0.1225	0.2414	0.5485
0.80	0.0163	0.0326	0.0813	0.1618	0.3163	0.6789
1.00	0.0203	0.0406	0.1012	0.2007	0.3880	0.7757
1.20	0.0243	0.0485	0.1210	0.2391	0.4559	0.8405
1.40	0.0283	0.0566	0.1407	0.2769	0.5195	0.8783
1.60	0.0323	0.0645	0.1604	0.3140	0.5783	0.8963
1.80	0.0363	0.0725	0.1799	0.3504	0.6320	0.9021
2.00	0.0403	0.0805	0.1993	0.3858	0.6804	0.9026
2.20	0.0443	0.0884	0.2186	0.4203	0.7234	0.9034
2.40	0.0483	0.0964	0.2377	0.4538	0.7609	0.9067
2.60	0.0523	0.1043	0.2567	0.4862	0.7933	0.9132
2.80	0.0563	0.1122	0.2755	0.5174	0.8205	0.9220
3.00	0.0602	0.1201	0.2942	0.5475	0.8430	0.9313
3.20	0.0642	0.1280	0.3126	0.5763	0.8612	0.9395
3.40	0.0682	0.1359	0.3309	0.6038	0.8754	0.9453
3.60	0.0722	0.1438	0.3490	0.6301	0.8861	0.9486
3.80	0.0762	0.1516	0.3668	0.6550	0.8940	0.9498
4.00	0.0802	0.1595	0.3844	0.6785	0.8990	0.9499
4.20	0.0841	0.1673	0.4018	0.7007	0.9028	0.9501
4.40	0.0881	0.1751	0.4189	0.7216	0.9047	0.9510
4.60	0.0921	0.1829	0.4358	0.7411	0.9057	0.9531
4.80	0.0966	0.1907	0.4524	0.7592	0.9060	0.9560
5.00	0.1000	0.1984	0.4688	0.7760	0.9061	0.9592

over the desired circle to obtain the fractional encircled energy. Particular attention was given to the problem of normalization. This hybrid approach provides accurate results for arbitrarily narrow spiders.

We also developed an intuitive empirical equation for the encircled energy based on Babinet's principle and Rayleigh's theorem. This empirical equation was then validated by comparison with rigorous solutions and used to study the parametric behavior of encircled energy for arbitrary spider configurations.

A. Empirical Equation Describing Spider-Diffraction Effects

The empirical equation is extremely simple. Given an annular aperture with a narrow opaque strut of

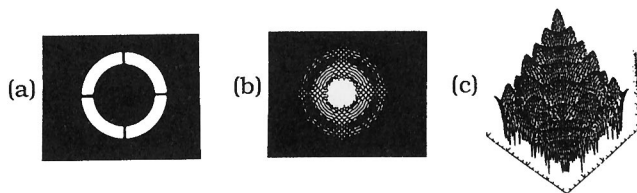


Fig. 8. (a) Annular aperture with a 0.7 obscuration ratio and four spiders whose width is 3% of the aperture diameter. (b) Corresponding PSF clearly showing complex interference effects. (c) Three-dimensional isometric plot of $I_n(x, y)$ on a log scale when determined by the first step of our hybrid approach to making rigorous calculations.

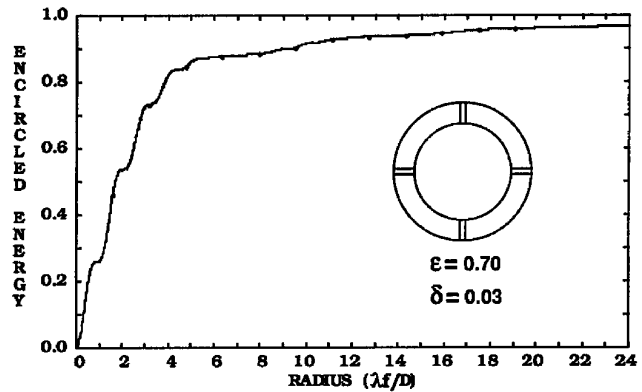


Fig. 9. Comparison of predictions from an empirical equation (continuous curve) with rigorous calculations (bold dots) indicating a less than 0.5% error.

rectangular cross section as shown in Fig. 5, the image consists of two parts. Part A is the image core that is just the diffraction-limited PSF caused by the annular aperture (diminished somewhat by the presence of the strut), and Part B is the diffraction flare caused by the strut. We ignore, for the moment, the interference effects that occur in the region in which these two functions overlap.

A consequence of Babinet's principle is that the Fraunhofer diffraction patterns of complementary apertures are identical except in the neighborhood of the center of the diffraction pattern.²¹⁻²³ Hence we know that the functional form of the diffraction pattern caused by the narrow strut (referred to as the diffraction flare) is identical to the Fraunhofer diffraction pattern caused by a thin rectangular aperture of width b and length a , i.e., $\text{sinc}^2(x_2 b / \lambda f) \text{sinc}^2(y_2 a / \lambda f)$. Furthermore the total energy contained in the flare (Part B) is proportional to area ab of the strut (Rayleigh's theorem applied to the complementary rectangular aperture). Clearly the presence of the strut also decreases the total energy passing through the aperture (by an amount proportional to its area, ab), and again, by Rayleigh's theorem, the total energy in the composite diffraction pattern is reduced by an equal amount.

If we ignore the interference effects that occur in the region in which these two functions overlap

Table 3. Validation of Empirical Equation

πr	Exact	Approx.	% Error
5	0.4593	0.4595	0.04
10	0.7306	0.7345	0.53
15	0.8450	0.8470	0.24
20	0.8747	0.8776	0.33
25	0.8820	0.8849	0.33
30	0.9013	0.9043	0.33
35	0.9258	0.9286	0.30
40	0.9333	0.9359	0.28
45	0.9365	0.9390	0.27
50	0.9446	0.9470	0.25
55	0.9522	0.9544	0.23

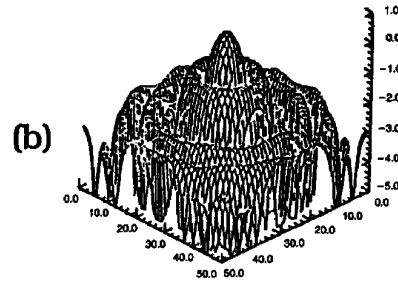
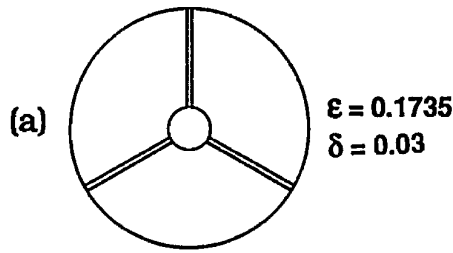


Fig. 10. Aperture configuration with small obscuration and three narrow spiders producing a relatively mild scalloping of the first few rings of the PSF.

(intuition tells us that the integration performed in calculating the encircled energy renders it insensitive to the exact nature of the interference pattern), the fractional encircled energy resulting from such an aperture can be written as

$$EE(r) = \frac{\int_{\phi=0}^{2\pi} \int_{r=0}^r \text{Part A } r dr d\phi + \int_{\phi=0}^{2\pi} \int_{r=0}^r \text{Part B } r dr d\phi}{\int_{x_2=0}^{\infty} \int_{y_2=0}^{\infty} (\text{Part A} + \text{Part B}) dx dy} \quad (18)$$

Because the presence of the strut both blocks energy from passing through the aperture and diffracts an equal amount out of the image core, we subtract an amount out of the core that is equal to twice the area of the strut, then add back in that small portion of the flare that lies inside the circle of interest and divide this numerator by the total energy that has been diminished by the area of the strut. When additional spiders are present, Part B becomes the sum of several diffraction flares; however, its fractional encircled energy does not change provided the spiders all have the same width. Because we have defined A_{annulus} as the area of the annulus and A_{spiders} as the area of all the spiders, we can merely

write

$$EE(r) = \frac{(A_{\text{annulus}} - 2A_{\text{spiders}})EE_{\text{annulus}}(r) + A_{\text{spiders}}EE_{\text{rect}}(r)}{A_{\text{annulus}} - A_{\text{spiders}}}, \quad (19)$$

where $EE_{\text{annulus}}(r)$ and $EE_{\text{rect}}(r)$ are the fractional encircled energy caused by an annular aperture and a narrow rectangular aperture, respectively.

When the annular aperture function shown in Fig. 6(a) is substituted into Eq. (10), the normalized irradiance distribution in the focal plane is shown to have the well-known analytic solution²⁴

$$I_n(x, y) = \frac{1}{(1 - \epsilon^2)^2} \left[\frac{2J_1(\pi r)}{\pi r} - \epsilon^2 \frac{2J_1(\epsilon \pi r)}{\epsilon \pi r} \right], \quad (20)$$

where ϵ is the linear obscuration ratio. The fractional encircled energy $EE_{\text{annulus}}(r)$ is thus easily calculated. Figure 6(b) illustrates this quantity graphically for a variety of obscuration ratios as a function of radius (in units of $\lambda f/D$). Table 1 provides the tabulated data making up the graph. Values of $EE_{\text{annulus}}(r)$ for any obscuration ratio can be obtained from this graph or table (directly or by interpolation) when the empirical equation is used to make encircled energy predictions in the presence of secondary mirror spiders.

Similarly, when the rectangular aperture function shown in Fig. 7(a) is substituted into Eq. (10), the normalized irradiance distribution in the focal plane has the analytic solution

$$I_n(x, y) = \text{sinc}^2(\delta x) \text{sinc}^2(\beta y), \quad (21)$$

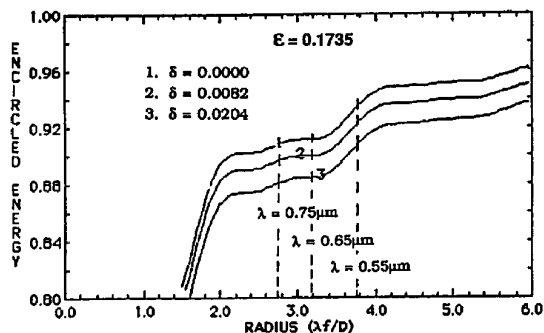


Fig. 11. Parametric plot of fractional encircled energy versus circle radius for different spider widths.

Table 4. Encircled Energy for Different Wavelengths and Spider Widths

λ (μm)	Encircled Energy in 25- μm Radius		
	$\delta = 0.0000$	$\delta = 0.0082$	$\delta = 0.0204$
0.55	0.9350	0.9219	0.9069
0.65	0.9115	0.8994	0.8842
0.75	0.9083	0.8960	0.8803

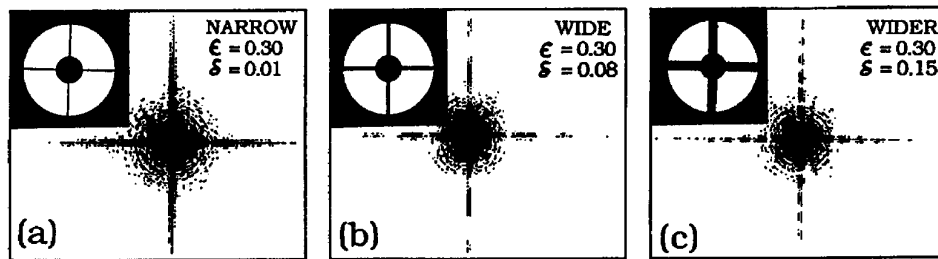


Fig. 12. Variations in the nature of the diffraction flares with spider width.

where $x = x_2 D / \lambda f$, $y = y_2 D / \lambda f$, and the fractional encircled energy from a narrow rectangular aperture (or opaque spider) is given by

$$EE_{\text{rect}}(r) = \beta \delta \int_{\phi=0}^{2\pi} \int_{r=0}^r \text{sinc}^2(\delta x) \text{sinc}^2(\beta y) r dr d\phi, \quad (22)$$

where $a = \beta D$ and $b = \delta D$ are the length and width of the rectangle, respectively. When $\delta \ll \beta$, this calculation can be approximated by the one-dimensional integral

$$EE_{\text{rect}}(r) \approx \beta \delta \int_{x=-r}^r \text{sinc}^2(\delta x) \text{sinc}^2(\beta y) dx. \quad (23)$$

This quantity is plotted in Fig. 7(b) for a variety of spider widths as a function of radius (in units of $\lambda f / D$). Table 2 provides the corresponding tabulated data.

Figures 6 and 7 can now be used as characteristic design or analysis curves for predicting encircled energy in the presence of secondary-mirror spiders by picking values of $EE_{\text{annulus}}(r)$ and $EE_{\text{rect}}(r)$ from these curves and plugging them into the empirical equation discussed above. Alternatively, Tables 1 and 2 can be used as look-up tables for the quantities $EE_{\text{annulus}}(r)$ and $EE_{\text{rect}}(r)$ when the empirical equation to make encircled energy predictions in the presence of secondary mirror spiders is used.

B. Validation of the Empirical Equation

Because our empirical equation for encircled energy ignores the interference between the image core and the diffraction flares, we chose an example where these effects are quite pronounced to compare the resulting predictions with rigorous calculations. Figure 8 shows a rather highly obscured ($\epsilon = 0.7$) annular aperture with four spiders whose width is 3% of the aperture diameter ($\delta = 0.03$) and a photograph of the resulting PSF that clearly shows the rather complex interference effects produced by these four subapertures.²⁵ Also illustrated in Fig. 8 is a three-dimensional isometric plot of $I_n(x, y)$ on a log scale as determined by the first step of our hybrid approach to making rigorous calculations. A careful comparison of this isometric plot and the photograph of the PSF indicates excellent qualitative agreement in detail.

The continuous curve in Fig. 9 is the fractional encircled energy prediction from our simple empirical

equation given by Eq. (19). The superimposed bold dots represent the rigorous calculations. Note from the tabulated data in Table 3 that the difference between the two methods is less than 0.5%. This is remarkably accurate for a method that ignores the prominent interference effects present in this example. However, the nature of the interference is such that it redistributes energy azimuthally but not radially. Hence, although integration of the diffraction pattern over a circle averages the azimuthal structure in the intensity distribution, it does not change its radially integrated value.

C. Parametric Encircled Energy Plots

For a much smaller obscuration ratio and three narrow spiders, the interference is less pronounced and the effects of spider diffraction show up as a relatively mild scalloping of the first few rings of the irradiance distribution in the focal plane as illustrated in Fig. 10.

For a 12.25-in.- (31-cm-) diam aperture with an obscuration ratio of 0.1735 and a 150-in. (381-cm) focal length, fractional encircled energy was predicted with the empirical equation and illustrated parametrically in Fig. 11 as a function of circle radius (in units of $\lambda f / D$) for spiders of three different widths. Note that for narrow spiders and modest circle sizes the curves run essentially parallel to one another. This parametric representation is particularly useful because one family of curves includes data for all wavelengths and circle sizes. For example, if one had a requirement for encircled energy in a given sized circle (i.e., 25- μm radius) for several different

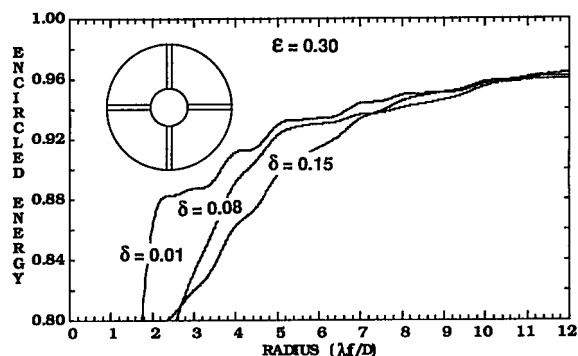


Fig. 13. Corresponding fractional encircled energy curves providing insight into the image-degradation effects of secondary mirror spiders of varying widths.



Fig. 14. Curved spider producing two searchlight beams emanating in opposite directions from the image core. This is intuitive if one approximates the curve as a set of straight segments.

wavelengths, the appropriate data points can be extracted from the graph and tabulated as shown in Table 4.

Figure 12 shows variations in the nature of the diffraction flares with spider width. Note the very broad central lobe of the sinc² function for very narrow spiders. This central lobe becomes narrower as the spider width increases, and considerable structure (many lobes) becomes evident for very wide spiders.

Because more light is diffracted into smaller angles by the wide spiders, the corresponding encircled energy curves shown in Fig. 13 do not remain parallel and can in fact cross one another. For example, if we compare the encircled energy of an annular aperture ($\epsilon = 0.3$) with four spiders that are narrow ($\delta = 0.01$), wide ($\delta = 0.08$), and very wide ($\delta = 0.15$), we see that the curve for the very wide spiders crosses that of the wide spiders at a radius of $\sim 2.6 \lambda f/D$ and crosses the curve for the narrow spiders at a radius of $\sim 11 \lambda f/D$.

There are also other interference effects apparent on close inspection of the diffraction patterns in Fig. 12. The double lines making up each lobe of the diffraction flare are real interference effects in the diffraction-limited PSF (not artifacts of the optics, detector, or film used to record the images). They are in fact Young's interference fringes produced by the two halves of the aperture separated by the spiders parallel to that diffraction flare.

D. Arbitrary Spider Shapes

Because our empirical equation for fractional encircled energy depends only on the spider width and the total area of the spiders, it can also be used with confidence for arbitrary spider shapes. Richter¹⁰ has discussed in some detail how a curved spider produces a searchlight effect (subtended angle = angle of arc) rather than the narrow diffraction flare produced by a straight spider. This is intuitive if one thinks merely of the curved spider as a set of straight segments, each of which produces a narrow diffraction flare perpendicular to the segment as illustrated in Fig. 14. As discussed above, the length of the flare depends only on the width of the spider, and because the fractional encircled energy of the individual flares are the same regardless of their orientation, the shape of a spider segment does not affect the encircled energy. Changing the orientation of a spider segment redistributes the diffracted energy only azimuthally, not radially. However, as discussed above, the total diffracted energy is proportional to the spider area and therefore its length.

If several curved spiders are designed to produce adjacent searchlight beams that neither have gaps nor overlap, presumably there would be no azimuthal variations in the resulting telescope PSF. Either three or four curved spiders produce this result if they can be combined to yield a semicircle and their relative orientation is correct. The single spider made from a section of pipe referred to above as a diffractionless mount and illustrated in Fig. 1 has a similar effect; however, the searchlight fans overlap by exactly 360 deg.

Thermal, structural, or dynamic considerations may determine the spider design or configuration for a given application; however, if fractional encircled energy is the image-quality requirement, the empiri-

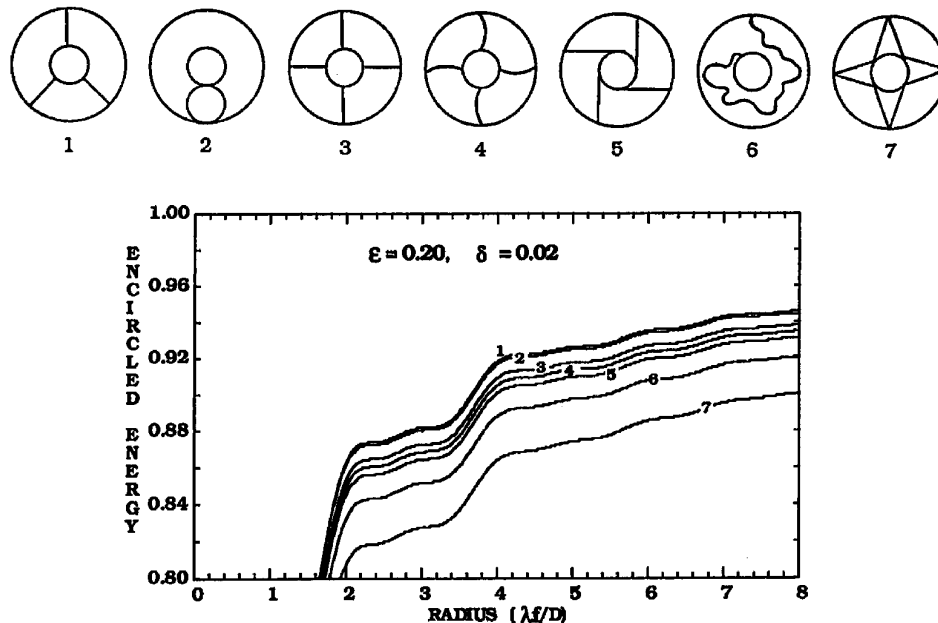


Fig. 15. Fractional encircled energy curves compared for a variety of spider configurations. The spider width is held constant.

cal equation presented in this paper can be used with confidence to compare the performance of candidate designs. The family of curves in Fig. 15 shows the encircled energy produced by the seven spider configurations illustrated. (Spider configuration 6 has no structural or practical merit and is included here only to emphasize that the image-quality degradation of truly arbitrary spider shapes can be evaluated by our empirical equation.) The width of the spiders and the central obscurations have been held constant for all configurations; hence the fractional encircled energy decreases with increasing total spider length.

Clark *et al.*¹² have presented an asymptotic approximation to the encircled energy for arbitrary aperture shapes that agrees well with rigorous calculations for the larger circle sizes. Figure 16 graphically shows a few discrete data points providing a detailed comparison between this asymptotic approximation, our empirical formula, and a rigorous calculation for an obscuration ratio $\epsilon = 0.5$ and four spiders of fractional width $\delta = 0.04$. The inset shows a comparison of the asymptotic approximation and an exact calculation over a wider range of the circle radii. Our empirical equation is considerably more accurate for the smaller circle sizes.

E. Other Obscurations and Particulate Contamination

Clearly the diffraction effects of obscurations other than secondary-mirror spiders can be predicted by a modified version of the simple empirical equation discussed above. The Hubble Space Telescope (HST) has three small circular pads that obscure the beam in addition to the central obscuration and four spiders. Equation (19) can be generalized to include the effect of these pads by merely adding a term to account for the pads:

$$EE_{\text{HST}}(r) = [(A_{\text{ann}} - 2A_{\text{spid}} - 2A_{\text{pad}})EE_{\text{ann}}(r) + A_{\text{spid}}EE_{\text{rect}}(r) + A_{\text{pad}}EE_{\text{circ}}(r)] / (A_{\text{aperture}}), \quad (24)$$

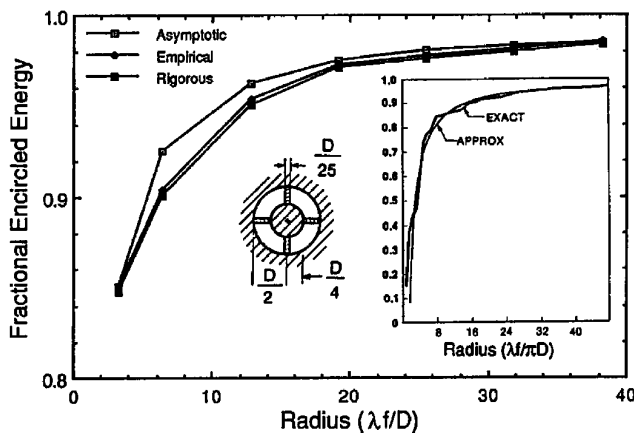


Fig. 16. Comparison of an asymptotic approximation, an empirical formula, and a rigorous calculation for a few discrete data points. The inset shows a comparison of the asymptotic approximation and an exact calculation over a wider range of circle radii.

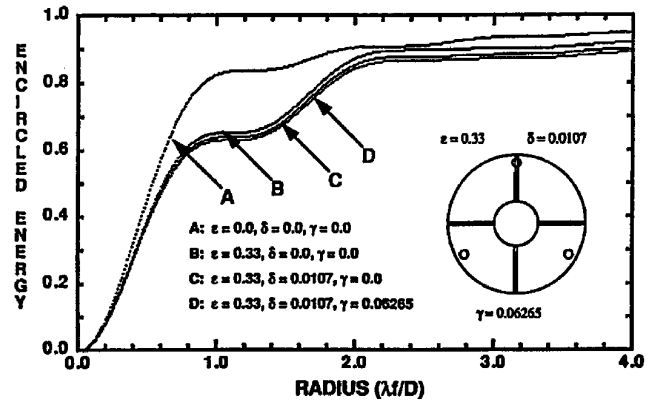


Fig. 17. HST aperture and diffraction-limited performance including the effects of central obscuration, spiders, and pads.

where

$$A_{\text{pad}} = M\pi\gamma^2D^2/4, \quad M = \text{number of pads} \quad (25)$$

is the area of the aperture covered by the pads and $EE_{\text{circ}}(r)$ is the fractional encircled energy of an unobscured circular aperture of diameter γD . The aperture configuration is shown in Fig. 17 along with the fractional encircled energy curves for A, an unobscured circular aperture; B, an annular aperture with an obscuration ratio of 0.33; C, an annular aperture with four secondary-mirror spiders of fractional width 0.0107; and finally D, the HST aperture complete with three small circular pads with fractional diameters of 0.06365.

Even the effects of particulate contamination (dust) on a telescope mirror can be modeled in this way. Parametric predictions of image degradation caused by particulate contamination of the HST primary mirror was calculated by generalizing Eq. (24) to include two extra terms:

$$EE_{\text{dust}}(r) = [(A_{\text{ann}} - 2A_{\text{spid}} - 2A_{\text{pad}} - 2A_{\text{dust}})EE_{\text{ann}}(r) + A_{\text{spid}}EE_{\text{rect}}(r) + A_{\text{pad}}EE_{\text{circ}}(r) + A_{\text{duct}}EE_{\text{dust}}(r)] / (A_{\text{aperture}}), \quad (26)$$

where A_{dust} is the area of the aperture covered by dust. $EE_{\text{dust}}(r)$ is the fractional encircled energy of the scattered light distribution caused by the dust. The value of $EE_{\text{dust}}(r)$ is unknown, but certainly negligible, because the dust is so small that its

Table 5. HST Image Degradation

Areal Dust Coverage	Fractional Encircled Energy	
	Case 1	Case 2
0.00	0.730	0.730
0.01	0.723	0.716
0.02	0.715	0.700
0.03	0.707	0.658
0.04	0.698	0.670
0.05	0.689	0.655

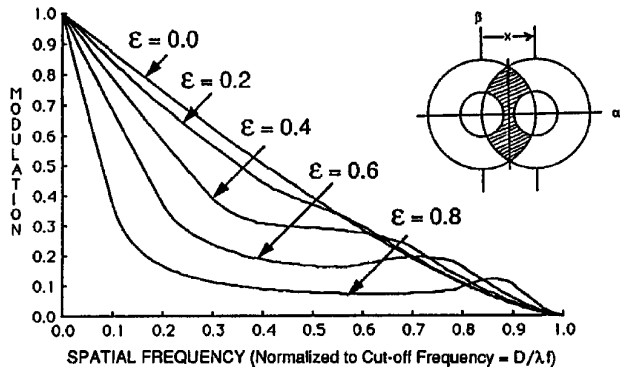


Fig. 18. MTF for an annular aperture with obscuration ratio ϵ .

diffracted/scattered light distribution is very broad compared with $\lambda f/D$.

We must be careful now because encircled energy is fractional quantity whose denominator can be proportional to the total energy reaching the focal plane:

$$A_{\text{aperture}} = A_{\text{ann}} - A_{\text{spid}} - A_{\text{pad}} - A_{\text{dust}}, \quad \text{Case 1,} \quad (27)$$

or it can be proportional to the total energy collected by a clean mirror:

$$A_{\text{aperture}} = A_{\text{ann}} - A_{\text{spid}} - A_{\text{pad}}, \quad \text{Case 2.} \quad (28)$$

Equation (26) was used to calculate the fractional encircled energy for both cases. A Strehl ratio of 0.906 was used to approximate the additional image-quality degradation caused by the maximum allowable rms wave-front error of 0.05 waves. We obtained the encircled energy predictions tabulated in Table 5. The denominator for Case 1 is reduced by dust and hence degrades the encircled energy substantially less than for Case 2. Case 2 permits only about half as much contamination as Case 1.

The HST image-quality requirement stated that 70% of the total energy reaching the focal plane from a stellar image must be contained within a radius of 0.10 arcsec (Case 1). Our predictions therefore indicate that the HST image-quality requirement can be satisfied with 3.8% areal dust coverage on the primary mirror.

5. Modulation Transfer Function

The modulation transfer function (MTF) is defined as the normalized autocorrelation of the pupil function as illustrated in Fig. 2. Closed-form analytical solutions for the MTF of annular pupil functions with narrow spiders are rather cumbersome for many

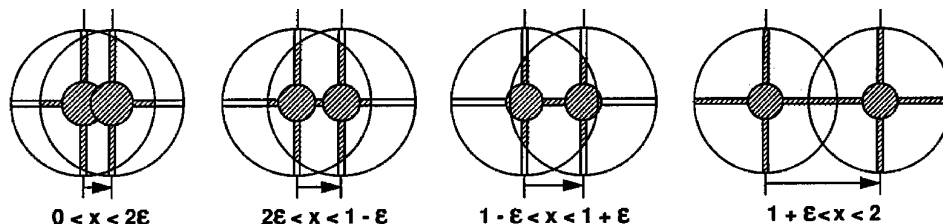


Fig. 19. Analytical solution for the MTF profile in the x direction ($\theta = 0$).

spider configurations. However, we encounter sampling problems when performing the alternative calculation with fast-Fourier-transform (FFT) routines:

$$\text{MTF} = \frac{\int_{-\infty}^{\infty} \int_{-\infty}^{\infty} f(\alpha, \beta) f(\alpha - x, \beta - y) d\alpha d\beta}{\int_{-\infty}^{\infty} \int_{-\infty}^{\infty} |f(\alpha, \beta)|^2 d\alpha d\beta}. \quad (29)$$

For a binary amplitude (opaque/transparent) diffracting aperture the numerator of the above equation is the area of overlap as a function of the shift parameter, and the denominator is just the total area A_T of the aperture²⁶:

$$\text{MTF} = \frac{R_{ff}}{A_T}, \quad R_{ff} = \int_{-\infty}^{\infty} \int_{-\infty}^{\infty} f(\alpha, \beta) f(\alpha - x, \beta - y) d\alpha d\beta. \quad (30)$$

For a circular aperture of diameter D , it is straightforward to show that¹⁷

$$\text{MTF} = \frac{(D^2/2)[\cos^{-1}(r/D) - (r/D)[1 - (r/D)^2]^{1/2}]}{\pi D^2/4}. \quad (31)$$

A. MTF of Annular Apertures

The closed-form analytical solution for the MTF of an annular aperture of outer diameter D_1 and inner diameter D_2 is now obtained by

$$\text{MTF} = \frac{R_{ff}}{\pi(D_1^2 - D_2^2)/4}, \quad (32)$$

where $R_{ff} = R_{f_1 f_1} - 2R_{f_1 f_2} + R_{f_2 f_2}$, where $R_{f_1 f_1}$ is the autocorrelation of the circle function defining the outer radius of the annulus, $R_{f_2 f_2}$ is the autocorrelation of the circle function defining the inner radius of the annulus, and $R_{f_1 f_2}$ is the cross-correlation of the two circles defining the inner and outer radii of the annulus.

Figure 18 illustrates the MTF of an annular aperture for several different obscuration ratios.

B. Analytic Solution of MTF with Spiders

Closed-form analytical solutions for the MTF of annular pupil functions with four narrow spiders

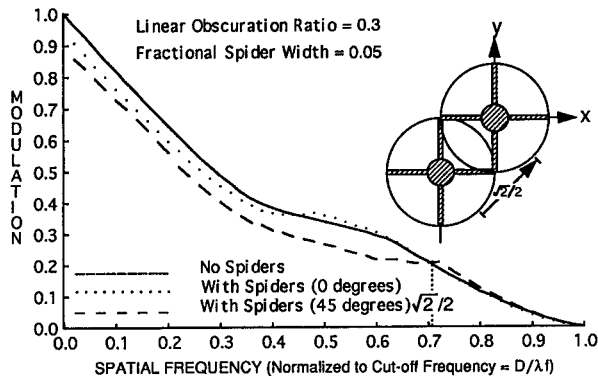


Fig. 20. Effect of telescope secondary mirror spiders on MTF. Note the improvement at high spatial frequencies.

have been obtained by breaking the autocorrelation integral of Eq. (30) into the sum of four different integrals:

$$R_{ff} = \int_{\alpha=0}^{2\epsilon} f(\alpha)f(\alpha-x)d\alpha + \int_{\alpha=2\epsilon}^{1-\epsilon} f(\alpha)f(\alpha-x)d\alpha + \int_{\alpha=1-\epsilon}^{1+\epsilon} f(\alpha)f(\alpha-x)d\alpha + \int_{\alpha=1+\epsilon}^2 f(\alpha)f(\alpha-x)d\alpha, \quad (33)$$

where the limits of integration are for an annulus with an outer radius of unity as illustrated in Fig. 19.

A similar closed-form integral can be solved for the MTF profile in the $\theta = 45^\circ$ direction. For an annular aperture with obscuration ratio $\epsilon = 0.30$ and fractional spider width $\delta = 0.05$ in Fig. 20 we compare these two MTF profiles with that for no spiders at all. Note that the presence of secondary-mirror spiders actually improves the MTF over certain spatial-frequency regimes. For example, it is readily shown that for spatial frequencies greater than $\sqrt{2}/2$ times the cutoff spatial frequency, the 45° profile is enhanced by the factor

$$A_{\text{ann}}/A_T = \frac{\pi D^2(1-\epsilon^2)/4}{\pi D^2(1-\epsilon^2)/4 - 2D^2\delta(1-\epsilon)} = 1.108. \quad (34)$$

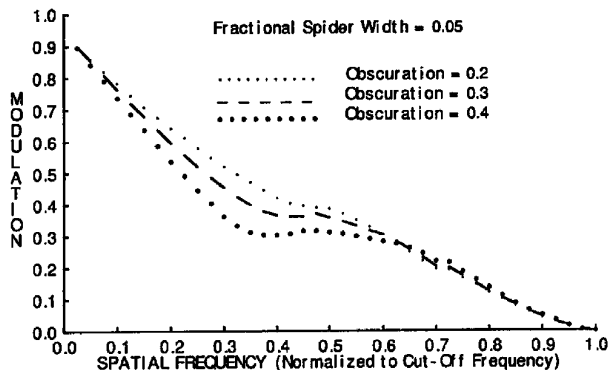


Fig. 21. Sensitivity of the MTF to the central obscuration ratio.

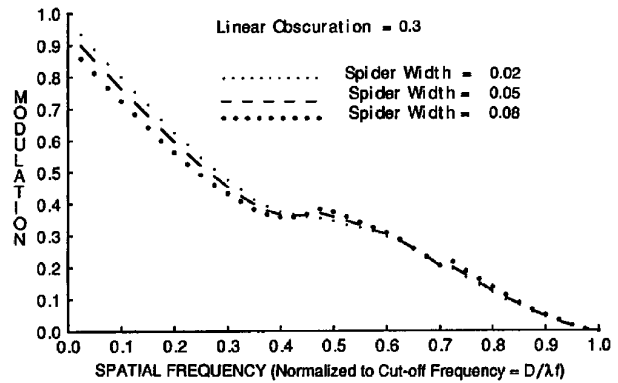


Fig. 22. Sensitivity of the MTF to the spider width.

The above relationship is restricted to the case of four narrow spiders in an annular aperture with obscuration $\epsilon \leq \sqrt{2} - 1$.

C. MTF Sensitivity Curves

Figures 21 and 22 show the sensitivity of the MTF to variations in the obscuration ratio and the spider width, respectively. In Fig. 21 we hold the spider width fixed at 5% of the aperture diameter and vary the obscuration ratio from 0.2 to 0.3 to 0.4. In Fig. 22 we hold the obscuration ratio fixed at $\epsilon = 0.3$ and vary the spider width from 2% to 5% to 8% of the aperture diameter.

Secondary mirror spiders thus have a significant but modest effect on the MTF, with an initial abrupt drop in the modulation at a very low spatial frequency. At high spatial frequencies, there is actually an increase in the MTF resulting from the normalization by the reduced area of the aperture.

6. Summary and Conclusions

We have shown that diffraction effects from secondary mirror spiders can significantly degrade telescope image quality; however, these effects vary drastically with the particular image-quality criterion. Rigorous analytical diffraction calculations are often unwieldy for complicated aperture shapes, and virtually all commercially available optical-design and analysis codes that have a diffraction analysis capability are based on numerical Fourier-transform algorithms that frequently lack adequate sampling density to model very narrow spiders. Scalar diffraction theory and Fourier techniques have been applied to model the effects of spider diffraction parametrically on the Strehl ratio (or the peak intensity of the diffraction image), the fractional encircled energy, and the MTF. Parametric performance predictions are presented as a function of the central obscuration ratio, the particular spider configuration, and the width of the spiders. In particular, when fractional encircled energy is the image-quality criterion of choice, a simple empirical equation is presented in this paper and validated to be remarkably accurate for arbitrary obscuration ratio and spider configurations.

The authors are grateful for the many useful comments and suggestions of the reviewers of the original manuscript of this paper. It is a much improved paper because of their conscientious efforts.

References and Notes

1. A. Couder, "Dealing with spider diffraction," in *Amateur Telescope Making, Advanced (Book Two)*, A. G. Ingalls, ed. (Scientific American, New York, 1946), pp. 260–262.
2. R. E. Cox, "Spider diffraction in moderate-size telescopes," *Sky Telesc.* 166–171 (Sept. 1960).
3. R. C. Ludden, "A 10-inch reflector fashioned in wood," *Sky Telesc.* 112–114 (Feb. 1969).
4. C. H. Werenskiold, "A note on curved spiders," *Sky Telesc.* 262–263 (Oct. 1969).
5. R. E. Cox, "Secondary mirrors and spiders," *Telesc. Making* 7, 4–7 (Spring 1980).
6. W. A. Rhodes, "An antidiffraction mask for reflectors," *Sky Telesc.* 289–290 (Apr. 1957).
7. Kenneth Novak & Co., *Catalog*, Box 69, Ladysmith, Wisc. 54848.
8. C. H. Werenskiold, "Improved telescope spider design," *J. R. Astron. Soc. Can.* 35, 268–273 (1941).
9. E. Everhart and J. Kantorski, "Diffraction effects produced by obscurations in reflecting telescopes of modest size," *Astron. J.* 64, 455–463 (1959).
10. J. L. Richter, "Spider diffraction: a comparison of curved and straight legs," *Appl. Opt.* 23, 1907–1913 (1984).
11. L. M. Beyer and L. C. Clune, "Intensity and encircled energy for circular pupils obscured by strut supported central obscurations," *Appl. Opt.* 27, 5067–5071 (1988).
12. P. P. Clark, J. W. Howard, and E. R. Freniere, "Asymptotic approximation to the encircled energy function for arbitrary aperture shapes," *Appl. Opt.* 23, 353–357 (1984).
13. P. J. Peters, "Aperture shaping—a technique for the control of the spatial distribution of diffracted energy," in *Stray Light Problems in Optical Systems*, J. D. Lytle and H. E. Morrow, eds., *Proc. Soc. Photo-Opt. Instrum. Eng.* 107, 63–69 (1977).
14. H. F. A. Tschunko and P. J. Sheehan, "Aperture configuration and imaging performance," *Appl. Opt.* 10, 1432–1438 (1971).
15. A. B. Meinel, M. P. Meinel, and N. J. Woolf, "Multiple aperture telescope diffraction images," in *Applied Optics and Optical Engineering*, R. R. Shannon and J. C. Wyant, eds. (Academic, New York, 1983), Vol. 9, pp. 149–201.
16. J. W. Goodman, *Introduction to Fourier Optics* (McGraw-Hill, New York, 1968), pp. 61, 113.
17. J. D. Gaskill, *Linear Systems, Fourier Transforms, and Optics* (Wiley, New York, 1978), pp. 194, 216.
18. H. H. Hopkins, *Wave Theory of Aberrations* (Oxford U. Press, New York, 1950), Chap. 2, p. 21.
19. R. Bracewell, *The Fourier Transform and its Applications* (McGraw-Hill, New York, 1965), p. 112.
20. A. A. Dantzler, "Encircled energy correction method for ray-trace programs," *Appl. Opt.* 27, 5001–5002, (1988).
21. M. Born and E. Wolf, *Principles of Optics* (Pergamon, Oxford, 1980), Chap. 8, p. 381.
22. E. Hecht, *Optics* (Addison-Wesley, Reading, Mass., 1987), Chap. 10, p. 458.
23. M. V. Klein, *Optics* (Wiley, New York, 1970), Chap. 7, p. 298.
24. H. F. A. Tschunko, "Imaging performance of annular apertures," *Appl. Opt.* 13, 1820–1823 (1974).
25. These photographs were provided by H. F. A. Tschunko, NASA/GSFC.
26. R. R. Butts and C. B. Hogge, "The modulation transfer function of an annular aperture with supporting struts," Air Force Weapons Laboratory report AFWL-TR-75-311 (Feb. 1976).